Synthesis and application of N_doped FeNi3/TiO2 nano-photocatalyst in advanced oxidation process to remove reactive red 195 dye from aqueous medium

Z. Sahebdadzehi
Birjand University of Medical Sciences
M. Khodadadi (maryam.khodadadi@gmail.com)
Birjand University of Medical Sciences
H. Dorri
Birjand University of Medical Sciences

Research Article

Keywords: N-dopedFeNi3/Tio2 nanocomposite, photocatalytic degradation, advanced oxidation, RR195 pollutant

Posted Date: March 23rd, 2022

DOI: https://doi.org/10.21203/rs.3.rs-1453184/v1

Abstract

Dyes are one of the most dangerous chemical compounds in industrial wastewater, including textile wastewater. Reactive dyes have many applications in the textile industry. Nevertheless, due to the high solubility and stability of these dyes in water, the discharge of wastewater containing these dyes to receiving waters prevents the transmission of sunlight to aquatic environments and disrupts biological processes. The aim of this study was to synthesize N_doped $FeNi_3/TiO_2$ nano-photocatalyst and to investigate the removal efficiency of reactive red 195 dye from aqueous medium. In this study, the effect of important variables was investigated including initial concentration including pH (3-11), contact time (5 - 200 minutes), dye concentration (5 - 40 mg l^{-1}), and nanocomposite dose (1 - 6 g l^{-1}), in removal of reactive red 195 dye. The characteristics of the synthesized nanocomposites were also studied using BET, FTIR, FESEM, and VSM techniques. The results of this study revealed that increasing the contact time and decreasing the dye concentration enhanced the adsorption efficiency. The highest percentage of RR 195 dye adsorption was 82% after 90 minutes at the adsorbent concentration of 4 g l^{-1}, pH=3 and the initial concentration of RR 195 of 5 mg l^{-1}. Detection techniques also confirmed the synthesis of good quality synthesized nanocomposites. According to the results, the advanced oxidation process of N-doped $FeNi_3/Tio_2$ nano-photocatalyst had a high efficiency removal of reactive red 195 dye adsorption from aqueous medium. As a result, this method can be used effectively in the treatment of colored wastewater.

1 Introduction

Many dyes are produced due to the waste and residuals of textile, dyeing, printing, rubber, paper, plastic, and related industries. Most dyes have aromatic rings in their structure making them highly toxic, non-biodegradable, carcinogenic, and mutagenic to the human body and aquatic animals (Yaman & Gündüz 2015). Meanwhile, in terms of dye production, the most important industries are usually the textile and dyeing industries (Somayajula et al. 2012).The textile industry is an important part of the industries of developing countries (Aksakal & Ucun 2010). About one-fifth of the total dye production in the textile industry is transferred to the environment through wastewater (Chládková et al. 2015). Dyes are classified into three main categories: anionic (direct, acidic and reactive), cationic (all primary colors), and non-ionic (dispersed colors) (Mahmoud et al. 2016). Azoic dyes are the largest group of dyes used for textile dyeing and other industrial applications (Mate & Pathade 2012). Dyes are chemical compounds that are important for a variety of reasons, including reduced light permeability and disrupted photosynthesis in water sources. Aesthetically, these compounds also negatively affect water quality and cause allergies, dermatitis, skin irritation, cancer, and genetic mutations in humans (Mahmoud et al. 2013). Reactive red 195 contains an active group consisting of an aromatic heterocyclic ring containing fluoride or chloride ions (Tahir et al. 2016). This dye is commonly used for dyeing cellulose fabrics and printing on fabric textures (Birmole et al. 2019).

Many aromatic color rings can affect the residues of various substances that are mutagenic, non-biodegradable, carcinogenic, and toxic to humans. Traditional methods cannot easily eliminate colors (Clavijo & Osma 2019). Thus, the removal of dye from industrial wastewater for environmental safety is challenging (Rani et al. 2017). Azo RR 195 dye is one of the dyes that includes the reaction group and is used in industries (Raval, Shah, Ladha, et al. 2016). There are various methods introduced as water treatment, such as Fenton, flocculation and adsorption processes, biological treatment, electrochemical techniques, ion exchange, advanced oxidation processes, and photocatalytic degradation under ultraviolet light (Rahimi et al. 2011). Advanced oxidation process or AOPs can be used in the decomposition of most organic and inorganic compounds without producing waste and problems with temperature and atmospheric pressure (Raval, Shah, & Shah 2016).

An important mediator produced in this process is reactive hydroxyl radicals (OH^{-}) which can support primary oxidants such as TiO_2, H_2O_2, UV, etc. In recent years, the use of magnetic nanoparticles as adsorbents to remove various contaminants has increased for RR 195 due to their important properties such as easy separation by an external magnetic field, easy synthesis, high surface area, and easy surface modification (Badruddoza et al. 2011). On the other hand, magnetic nanoparticles have challenges that prevent applications such as rapid aggregation, oxidation, etc. (Solisio & Aliakbarian 2017).

One way to mitigate such challenges is to use a composite shell structure to preserve the core and magnetic properties of $FeNi_3$ as well as other iron alloys. When an insulating shell is used, nanocomposites in RR red 195uce the performance, stability and aggregation of nanoparticles and RR red 195 their toxicity (Zhu et al. 2018). On the other hand, the special properties of TiO_2 as a cost-effective, non-toxic, and stable nanoparticle for a long time can be used as a catalyst to purify water and eliminate air pollution (Farooghi et al. 2018). Studies have shown that doping non-metals such as nitrogen (N), carbon (C), sulfur (S), and fluorine (F) with Tio_2 would lower the recombination property and improve the photocatalytic activity of this particle under visible light with a wavelength greater than 400 nm (Ho et al. 2006). Among these non-metals, nitrogen is important due to its low ionization energy, similar size to oxygen, and high stability (Asahi et al. 2001). In the created structure, nitrogen ions replace oxygen ions in the Tio_2 lattice and create a new energy level in the Tio_2 bond gap, reducing the electron-hole recombination property (Huang et al. 2007). The process of TiO_2 oxidation begins with the exchange of adsorption and diffusion (Lu et al. 2011). The photocatalytic limitations of TiO_2 are due to the small surface area and low adsorption properties. Formation of different composites and hybrids can cover these limitations thus enhancing their efficiency and reverse degradation (Liu et al. 2005). In general, TiO_2 interacts with metal ions in oxidation radicals to reduce oxidation and improve the light absorption spectrum. In addition, metal ions help reduce electron hole recombination by trapping electrons (Nasseh, Taghavi, et al. 2019). In addition, as shown in our previous studies (Khodadadi et al. 2019), the significant degradation efficiencies of organic pollutants using Fe-Ni_3/TiO_2 indicate the good potential of this technique as a real wastewater treatment system of an oil refinery. The results revealed that the combination of iron with Ni_3 can turn it into a photocatalyst (Nasseh et al. 2018). In the present paper,

$FeNi_3$ magnetic nanoparticles have been fabricated using nickel and iron salts (Eslami et al. 2016; Nasseri & Sadeghzadeh 2013) and N-dopped in the Fe-Ni_3/TiO_2 synthesized structure. Its photocatalytic activity to remove RR 195 from aqueous solution in the presence of visible light has been examined (Kamranifar et al. 2018; Nasseh, Barikbin, et al. 2019).

2 Materials And Methods

2.1 Chemicals

The dye used in this study was a dye (RR195) solution with a molecular weight of 1136.32 and molecular formula of $C_{31}H_{19}C_lN_7Na_5O_{19}S_6$ (Tan et al. 2012). A spectrophotometric device with a wavelength of 540 nm was used to measure the residual dye concentration (Birmole et al. 2019).

Other materials used included hydrazinium hydrate with formula $N_2H_4.H_2O$ with 80% purity, ethanol (C_2H_5OH), titanium butoxide (TBOT) with formula $C_{12}H_{28}O_4Ti$, iron chloride with formula FeCl2 ($4H_2O$), hydrogen peroxide 1 gr, 6% w Nickel $NiCL_2$ ($6H_2O$), HCl, and NaOH all produced by Merck. Dionysian water was used to prepare the solutions. The method described in Standard Method Book No. 5220 was employed for measurement (Clesceri et al. 2012).

The devices used included spectrophotometer (model (UV/Vis T80 $^+$, FTIR (model AVATAR 370 made in USA with spectrometer in the range of (400–4000 cm), FESEM (model SLGMA Vp-500 Zeiss made in Germany) and VSM (model LAKE shore 7404 made in USA). BET analysis was performed by using model device (BElSORP Mini, Microtrac Bel Corp).

2.2 N_doped $FeNi_3/TiO_2$ composite synthesis method

2.2.1 Synthesis of Fe-Ni_3

Initially, 1 gram of polyethylene glycol 6000 was dissolved in 180 ml of ion-free water. Then 0.713 g of nickel chloride and 0.198 g of iron chloride were dissolved separately in two containers containing 30 ml of ion-free water and added to the first solution. After complete mixing, using sodium hydroxide, the pH of the solution was adjusted between 12 and 13, then 9.1 ml of hydrazine hydrate ($N_2H_4.H_2O$) with a concentration of 80% was added to the obtained suspension. The reaction was carried out for 24 hours at room temperature and the pH was constantly monitored during this time to maintain the desired range. Finally, the obtained $FeNi_3$ nanocomposite was rinsed with water and ethanol in several steps. This nanocomposite was dried in a vacuum oven at 30°C after separation by an external magnetic field (Khodadadi et al. 2019; Nasseh et al. 2018; Nasseh, Taghavi, et al. 2019).

2.2.2 Synthesis of Fe-Ni_3/TiO_2 nanocomposite

Here, 0.2 g of the synthesized $FeNi_3$ magnetic nanoparticles was mixed in a mixture containing 10 ml of 1-propanol and 50 ml of deionized water. Then, 2 ml of titanium butoxide (TBOT) was added dropwise to

the previous solution and added for 24 hours while the resulting mixture was stirred at 500 rpm at 80°C. Finally, the obtained $FeNi_3/TiO_2$ nanocomposite was rinsed with water and ethanol in several steps. This nanocomposite was dried in a vacuum oven at 30°C after separation by an external magnetic field. Once dried, the samples were placed in a 400 ° C oven for 4 hours for calcination (Lian et al. 2009).

2.2.3 Synthesis of N-doped Fe-Ni_3/TiO_2 catalyst

Initially, 140 mg of $FeNi_3/TiO_2$ was dispersed in 70 ml of deionized water for 20 minutes under ultrasonic waves. Then with 35% ammonia, the pH was adjusted to 10 and then 2 ml of hydrazine hydrate was added and stirred. Finally, it was heated in a Teflon autoclave at 80°C for 3 hours. Then, the reduced sheets of N_doped $FeNi_3/TiO_2$ were collected and the product was washed with deionized water and dried it in a vacuum oven at 50 ° C (Wang et al. 2012; Wang et al. 2013).

2.2.4 Investigation of Fe-Ni_3/TiO_2 nanocomposite properties

FESEM Images were used to determine the shape, mean diameter, and surface area of the synthesized nanoparticles. The magnetic properties of the nanoparticles were measured using a VSM vibrating sample magnetometer analysis. Also, X-ray spectra, FTIR, and BET were used to identify the composition and crystalline structure characteristics of RR 195 and nanoparticle size.

3 Rr 195 Removal Steps By N-doped Fe-ni/tio Catalyst

3.1 Adsorption of RR 195 by N-doped Fe-Ni_3/TiO_2 catalyst

A stock solution (1000 mg L^{-1}) of RR 195 dye was made in deionized water. The effect of different adsorption parameters of RR 195 by nanoparticles was investigated. Five pH ranges (Cai et al. 2021; Kim et al. 2013) were used including (3, 5, 7, 9, 11) for reactive red 195 dye, five initial concentration ranges for the desired contaminant (5-10-20-30-40 mg L^{-1}), nine ranges for contact time (5, 10, 15, 30, 60, 90, 120, 180, 200 minutes), and four ranges of nanocomposite (1-2-4 and6 g l^{-1}) with N42 magnet employed to separate the magnetic nanoparticles. RR 195 concentration was measured before and after the adsorption process using a spectrophotometer at a wavelength of 547 nm. In all stages of the experiments, the efficiency and adsorption capacity in the adsorption stage were calculated using the following equations.

To calculate the removal efficiency, Eq. 1 was used, where %R represents the removal efficiency, Ct denotes the residual concentration of reactive red 195 dye at time t (mg L^{-1}), and C0 is the initial concentration of dye (mg L^{-1}).

$$\%R = C_{0-C_t} / c_0 \times 100$$

1

Equation 2 was used to calculate the equilibrium adsorption capacity.

$$qe = V/M \times \left(C_1 \_ C_T\right)$$

2

C_1 and C_t are the initial concentration and the residual concentration at time t in mg L^{-1}, q_e represents equilibrium capacity in mg/g, V is the volume of the solution in lit, and M indicates the dose of the adsorbent in gram (Tang et al. 2017).

To determine the pH_{ZPC} or zero-point pH for N-doped $FeNi_3/Tio_2$ magnetic nanoparticles, 100 ml of deionized water was added to the Erlenmeyer flask. The pH of the deionized water was then adjusted within the range of 2–12 with hydrochloric acid and 0.1 N sodium hydroxide. Next, 0.1 g L^{-1} of magnetic nanoparticles was added to each of the desired containers and placed on a shaker at a speed of 150 rpm. After 24 hours, the final pH of the solution was measured using a pH meter. The initial pH diagram was plotted against the final pH, and the point where the two RR 195 curves used each other indicated the isoelectric point (Khaniabadi et al. 2018; Panahi et al. 2019).

3.2 Adsorption isotherms, adsorption kinetics, and thermodynamics

The adsorption isotherms for RR 195 use the adsorption capacity of various adsorbents to evaluate the feasibility of a process and are also useful for analysis as well as design (Khaniabadi et al. 2017). In a system, the content of adsorbate per unit mass of adsorbent in RR 195 decreases with ease of concentration in RR 195. However, this relationship is not linear. Adsorption isotherms show the ratio between the concentration of the adsorbate unit and the compound concentration of the residual material in the solution. Adsorption isotherms can take many forms for different systems. In this study, two isotherm models known as Langmuir and Freundlich were evaluated. The Langmuir isotherm model describes the monolayer coating of the adsorbed compound on the adsorbent surface. Freundlich isotherm is based on monolayer and heterogeneous adsorption of adsorbate on adsorbent. Indeed, in the Freundlich model, it is assumed that the adsorption is monolayer and non-uniform. The following equation represents the Freundlich isotherm model. Eq. 3 was used to calculate the Freundlich isotherm.

$$qe = k_f c_e^{1/n} \quad (3)$$

In the Langmuir adsorption isotherm, adsorption is monolayer and the adsorption regions on the surface of the adsorbent are uniform, and all have the same adsorption power. Adsorption bonds are also reversible. The following equation represents the Langmuir isotherm model (Wanyonyi et al. 2014). Equation 4 was used to calculate the Langmuir isotherm.

$$c_e / q_e = 1 / q_{max} k_l + c_e / q_{max}$$

4 Results And Discussion

4.1 Characteristics of synthesized N-doped Fe-Ni_3/TiO_2 nanocomposite

4.1.1 FTIR analysis

FTIR spectroscopy was used to determine the functional groups of N-doped $FeNi_3/Tio_2$ magnetic nanocomposite. Figure 1 displays the desired spectrum.

The presence of a peak at 494 cm^{-1} is related to the tensile vibrations of Fe-Ni, Ni-Fe-Ni, and Fe-Ni-Ni. The presence of a peak at 1347.73 cm^{-1} is related to C-H and N-O vibrations due to the residue of some raw materials such as hydrazine hydrate during manufacturing. The adsorption band at 3937.85 cm^{-1} is associated with the vibrations of the hydroxyl functional group (O-H) in the sample due to the presence of moisture or water during adsorption. The FT-IR spectrum of Fe-Ni_3/TiO_2 indicates that TiO_2 is well coated on the $FeNi_3$ surface. The vibration peaks at 792 cm^{-1} and 1102 cm^{-1} have been assigned to the Ti-O-Ti bond. The broad peak appearing at 3819 cm^{-1} is due to the tensile vibration of the O-H bond. On the other hand, the vibrations of 1626, 675, and 590 cm^{-1} confirm the presence of shell on the surface of $FeNi_3$ nanoparticles. Also, the FTIR spectrum of the first Fe-Ni_3/TiO_2 N-doped nanocomposite at 667 was assigned to the presence of oxidized nitrogen such as Ti-O-N. The compact and broad band at the low wave number range between 1078 and 964 cm^{-1} was attributed to the strong tensile vibrations of the Ti -O and Ti -O-Ti bonds, indicating that the distance between the TiO2 band and N doping was reduced.

4.1.2 FESEM analysis

Scanning electron microscope (FESEM) was used to study the shape, surface, and average grain diameter, with Fig. 2 presenting the corresponding FESEM image. According to the figure, it can be found that N-doped $FeNi_3/Tio_2$ particles have aggregation properties which is due to their magnetic nature, causing the particles to adsorb each other well. Also, the closer it is taken from the surface to the material, the more its shape has not changed that. This is due to their amorphous state, because in different modes of the image, the shapes have not changed, so a regular structure is not recommended for it. The size of magnetic nanoparticles is within 33.5-67.31 nm and the texture of the material is dense in terms of compressibility, which indicates its high density.

4.1.3 VSM analysis

To determine the magnetic properties of the synthesized magnetic nanocomposite, a magnetic measuring device was used and the sample vibration (VSM) was measured at room temperature.

Figure 3 indicates that in the first step where the $FeNi_3$ nanoparticle was synthesized, its magnetization was 5 emu g^{-1}. In the next stage of synthesis ($FeNi_3/TiO_2$), its magnetization increased to 7 emu g^{-1}. The synthesized adsorbent was dispersed and could be dispersed again. These particles had also good magnetization in the N-doped $FeNi_3/Tio_2$ phase, indicating the potential use of a magnetic adsorbate which can be easily separated using an external magnet.

4.1.4 BET analysis

BET analysis was employed to measure the specific surface area of $FeNi_3/TiO_2$ N-doped magnetic nanocomposite with its results presented in Table 1. Its effective surface area is 112.42 m^2g^{-1}, considering that the specific surface area and total pore volume of N-doped $FeNi_3/TiO_2$nanoparticles are suitable therefore, it is expected to have good adsorption activity.

Table 1
Information on BET analysis of N-doped $FeNi_3/TiO_2$ nanocomposite

Nanoparticle	Surface area (m^2 g^{-1})	Average pore diameter (nm)	Pore volume (cm^3 g^{-1})
N-doped FeNi3/Tio2	112.48	7.7477	o.2186

4.2 Effect of different parameters on RR 195 adsorption on Fe-Ni_3/TiO_2 N-doped nanocomposite

4.2.1 Effect of pH

pH is an important factor in adsorption processes which can affect the surface load of the adsorbent. pHzpc of the synthesized nanocomposite was estimated before the adsorption test. The data show that the pzc pzc of N-doped Fe-Ni_3/TiO_2 nanocomposite was approximately 7.2. RR 195 is an anionic color, which is also used as an acid and alkaline marker (Munagapati & Kim 2017; Ojedokun & Bello 2017; Prasad et al. 2017). Figure 4 displays the effect of pH on the effectiveness and adsorption capacity of RR 195 using N-doped Fe-Ni_3/TiO_2 nanocomposite. As shown in the figure, in RR 195, which lowers the pH from 3 to 11, the removal efficiency has decreased. This is related to the adsorbent pHzpc, pKa, and the ionic structure of RR 195. pHzpc is a parameter used in adsorption studies and indicates the point at which the adsorbent surface charge is zero. If solution pH < pHzpc, the adsorbent surface charge is positive, if solution pH > pHzpc, the adsorbent surface charge is negative, and if pH = pHzpc, the adsorbent surface has no charge (positive and negative charges are equal) (Mohammadi & Aliakbarzadeh Karimi 2017; Taqui et al. 2017). Thus, with increasing pH, the electrostatic attraction force between the adsorbent and RR 195 diminishes and the adsorption efficiency in RR 195 decreases due to the anionic color property of RR 195. In the study, the highest removal percentage is related to pH of 3, where adsorbent surface charge is positive.

4.2.2 Effect of N-doped Fe-Ni_3/TiO_2 nanocomposite dose

As depicted in Fig. 5, regarding the effect of the concentration of N-doped Fe-Ni_3/Tio_2 nanocomposite (1–2-4-6 g L^{-1}) on the removal of RR 195, elevation of the concentration of adsorbent has enhanced the removal of RR. The efficiency increased due to the growth in the number of nanocomposites and the availability of more adsorption sites. An important factor in our studies is eliminating the effect of dose concentration at certain times. The results of this study can be consistent with studies conducted by Khani Abadi et al., which are related to the removal of RR 195 using activated carbon and montmorillonite (Wanyonyi et al. 2014).

4.2.3 Effect of concentration of RR 195

Figure 6 indicates the content of RR 195 adsorbed by the synthesized nanoparticles. This figure shows that as the initial concentration of RR 195 dye increases, its adsorption decreases due to the rise in the number of dye molecules to bind to the surface and thus the saturation of the adsorption sites on the adsorbent surface. On the other hand, the adsorption of RR 195 was rapid in the early stages and then slowed down as there are fewer binding sites on the adsorber surface to absorb the dye. Also, in a study conducted by Lambropoulou et al. on the removal of red reactive dye 195 by TiO_2 nanoparticles, it was shown that the removal percentage increased at lower concentrations (Chládková et al. 2015).

4.2.4 Isotherm absorption and kinetics studies

The most important parameter in the adsorption method is the study of adsorption isotherms expressing the adsorbent capacity and adsorbent concentration. Table 2 reports the results for the isotherm parameters for the adsorption of the red reactive dye 195 by N-doped$FeNi_3/Tio_2$. Based on the results, the adsorption isotherm follows the Langmuir model, which shows the graph of Ce versus Ce/qe. Since the value of R^2 was 0.97 for the Langmuir model and 0.93 for the Freundlich model, the adsorption isotherm follows the Langmuir model. Figure 7 displays the study of the Langmuir isotherm model on the adsorption of reactive red 195 with N-doped $FeNi_3/Tio_2$ magnetic nanocomposite. Kuleyin et al.'s (2011) study on the adsorption isotherm of Remazol Brillant Bhue R and Remazol Yellow dyes by surfactant-modified natural zeolite showed that the obtained data are more consistent with the Langmuir isotherm model (Kuleyin & Aydin 2011).

Table 2
Constants of the isotherm model of reactive red 195 dye adsorption by $FeNi_3/TiO_2$ magnetic nanocomposite

Langmuir isotherm			Freundlich isotherm		
R^2	q_{max} (mg g^{-1})	B (L mg^{-1})	R^2	N	K_f (mg g^{-1})
0.97	0.35	35.58	0.93	1.74	1.73

Table 3 lists the kinetic parameters of 195-N-dopedFeNi_3/Tio_2 reactive red dye adsorption. The pseudo-first-order kinetics model is obtained by plotting ln (qe-qt) versus t and quadratic kinetics in terms of t/qt versus t (Fig. 8). The first-order kinetic graph is used to obtain the coefficient R^2 and the constant value K_1, while the second-order kinetic graph is used to obtain k_2 and qe which is obtained by calculating the slope of the curve and the intercept. In this study, considering that in pseudo-second-order kinetics, the value of R^2 was equal to 0.99, so it follows the pseudo-second-order model. In a study by Raghunath et al. on the removal of textile dyes from industrial wastewater by the polymer nanocomposite of the amino acid proline, it was shown that isotherms obtained from different concentrations of adsorbent on dye adsorption kinetics followed a pseudo-second-order model .

Table 3
Kinetic parameters of reactive red 195 dye adsorption using $FeNi_3$/TiO_2 magnetic nanocomposite

pseudo-first-order kinetics			pseudo-second-order kinetics		
R^2	q_e(mg g^{-1})	K_1(min^{-1})	K_2(min^{-1})	q_e(mg g^{-1})	R^2
0.507	2.8	0.047	0.026	17.95	0.999

5 Conclusion

Examination of the effect of pH revealed that the highest percentage of removal of reactive red 195 dye was observed at pH 3 (82%). In this study, it was found that elevation of the initial concentration of reactive red 195 dye reduced the efficiency in the adsorption process by N-doped $FeNi_3$/TiO_2. The results of the optimal dose of nanocomposite indicated that the efficiency was enhanced with increasing the dose in the adsorption stage, but then the efficiency dropped due to the turbidity caused by the nanocomposite dose. The results of the N-doped $FeNi_3$/TiO_2 reactive red dye adsorption process indicated that the adsorption isotherm was consistent with the Langmuir model and the adsorption process followed pseudo-second-order kinetics. Based on the results, the synthesized N-doped $FeNi_3$/TiO_2 magnetic nanocomposite has a high ability to remove the reactive red 195 dye and can be used as a suitable and available nanocomposite.

Declarations

Data availability statement

The authors have no competing interests to declare that are relevant to the content of this article.

Declaration of Competing Interest

The authors declare that they have no known competing financial interests or personal relationships that could have appeared to influence the work reported in this paper.

Acknowledgments

The authors gratefully acknowledge the support of this work by Birjand university of Medical sciences.

Author contributions Statement

Sahebdadzehi and Dorri carried out the experiment. Sahebdadzehi wrote the manuscript with support from Khodadadi and Dorri. Sahebdadzehi fabricated the N-doped FeNi3/TiO2 magnetic nanocomposite and Khodadadi helped supervise the project. Dorri and Khodadadi conceived the original idea. Khodadadi supervised the project.

References

1. Aksakal O, Ucun H (2010) Equilibrium, kinetic and thermodynamic studies of the biosorption of textile dye (Reactive Red 195) onto Pinus sylvestris L. J Hazard Mater 181(1–3):666–672
2. Asahi R, Morikawa T, Ohwaki T, Aoki K, Taga Y (2001) Visible-light photocatalysis in nitrogen-doped titanium oxides. Science 293(5528):269–271
3. Badruddoza A, Tay A, Tan P, Hidajat K, Uddin M (2011) Carboxymethyl-β-cyclodextrin conjugated magnetic nanoparticles as nano-adsorbents for removal of copper ions: synthesis and adsorption studies. J Hazard Mater 185(2–3):1177–1186
4. Birmole R, Parkar A, Aruna K (2019) Biodegradation of Reactive Red 195 By A Novel Strain Enterococcus casseliflavus RDB_4 Isolated from Textile Effluent.Nature Environment & Pollution Technology18(1)
5. Cai A, He H, Zhang Q, Xu Y, Li X, Zhang F et al (2021) Synergistic Effect of N-Doped sp2 Carbon and Porous Structure in Graphene Gels toward Selective Oxidation of C–H Bond. ACS Appl Mater Interfaces 13(11):13087–13096
6. Chládková B, Evgenidou E, Kvítek L, Panáček A, Zbořil R, Kovář P et al (2015) Adsorption and photocatalysis of nanocrystalline TiO2 particles for Reactive Red 195 removal: effect of humic acids, anions and scavengers. Environ Sci Pollut Res 22(21):16514–16524
7. Clavijo C, Osma JF (2019) Functionalized leather: A novel and effective hazardous solid waste adsorbent for the removal of the diazo dye congo red from aqueous solution. Water 11(9):1906
8. Clesceri L, Greenberg A, Eaton A (2012) In: EW R (ed) Standard methods for the examination of water and wastewater. Publication Office, Washington DC
9. American Public Health Assosiation
10. Eslami A, Amini MM, Yazdanbakhsh AR, Mohseni-Bandpei A, Safari AA, Asadi A (2016) N, S co-doped TiO2 nanoparticles and nanosheets in simulated solar light for photocatalytic degradation of non-steroidal anti-inflammatory drugs in water: a comparative study. J Chem Technol Biotechnol 91(10):2693–2704

11. Farooghi A, Sayadi MH, Rezaei MR, Allahresani A (2018) An efficient removal of lead from aqueous solutions using FeNi3@ SiO2 magnetic nanocomposite. Surf Interfaces 10:58–64
12. Ho W, Jimmy CY, Lee S (2006) Synthesis of hierarchical nanoporous F-doped TiO 2 spheres with visible light photocatalytic activity.Chemical Communications(10):1115–1117
13. Huang Y, Zheng X, Zhongyi Y, Feng T, Beibei F, Keshan H (2007) Preparation of nitrogen-doped TiO2 nanoparticle catalyst and its catalytic activity under visible light. Chin J Chem Eng 15(6):802–807
14. Kamranifar M, Khodadadi M, Samiei V, Dehdashti B, Sepehr MN, Rafati L et al (2018) Comparison the removal of reactive red 195 dye using powder and ash of barberry stem as a low cost adsorbent from aqueous solutions: Isotherm and kinetic study. J Mol Liq 255:572–577
15. Khaniabadi YO, Basiri H, Nourmoradi H, Mohammadi MJ, Yari AR, Sadeghi S et al (2018) Adsorption of congo red dye from aqueous solutions by montmorillonite as a low-cost adsorbent. International journal of chemical reactor engineering 16(1)
16. Khaniabadi YO, Mohammadi MJ, Shegerd M, Sadeghi S, Saeedi S, Basiri H (2017) Removal of Congo red dye from aqueous solutions by a low-cost adsorbent: activated carbon prepared from Aloe vera leaves shell. Environ health Eng Manage J 4(1):29–35
17. Khodadadi M, Al-Musawi TJ, Kamranifar M, Saghi MH, Hossein Panahi A (2019) A comparative study of using barberry stem powder and ash as adsorbents for adsorption of humic acid. Environ Sci Pollut Res 26(25):26159–26169
18. Kim JR, Santiano B, Kim H, Kan E (2013) Heterogeneous oxidation of methylene blue with surface-modified iron-amended activated carbon
19. Kuleyin A, Aydin F (2011) Removal of reactive textile dyes (Remazol Brillant Blue R and Remazol Yellow) by surfactant-modified natural zeolite. Environ Prog Sustain Energy 30(2):141–151
20. Lian L, Guo L, Wang A (2009) Use of CaCl2 modified bentonite for removal of Congo red dye from aqueous solutions. Desalination 249(2):797–801
21. Liu W, Zhong W, Jiang H, Tang N, Wu X, Du W (2005) Synthesis and magnetic properties of FeNi3/Al2O3 core-shell nanocomposites. Eur Phys J B-Condensed Matter Complex Syst 46(4):471–474
22. Lu X, Liang G, Sun Q, Yang C (2011) High-frequency magnetic properties of FeNi3–SiO2 nanocomposite synthesized by a facile chemical method. J Alloys Compd 509(16):5079–5083
23. Mahmoud ME, Nabil GM, El-Mallah NM, Bassiouny HI, Kumar S, Abdel-Fattah TM (2016) Kinetics, isotherm, and thermodynamic studies of the adsorption of reactive red 195 A dye from water by modified Switchgrass Biochar adsorbent. J Ind Eng Chem 37:156–167
24. Mahmoud MS, Farah JY, Farrag TE (2013) Enhanced removal of Methylene Blue by electrocoagulation using iron electrodes. Egyptian J Petroleum 22(1):211–216
25. Mate MS, Pathade G (2012) Biodegradation of CI Reactive Red 195 by Enterococcus faecalis strain YZ66. World J Microbiol Biotechnol 28(3):815–826

26. Mohammadi A, Aliakbarzadeh Karimi A (2017) Methylene blue removal using surface-modified TiO2 nanoparticles: a comparative study on adsorption and photocatalytic degradation. J Water Environ Nanatechnol 2(2):118–128
27. Munagapati VS, Kim D-S (2017) Equilibrium isotherms, kinetics, and thermodynamics studies for congo red adsorption using calcium alginate beads impregnated with nano-goethite. Ecotoxicol Environ Saf 141:226–234
28. Nasseh N, Barikbin B, Taghavi L, Nasseri MA (2019) Adsorption of metronidazole antibiotic using a new magnetic nanocomposite from simulated wastewater (isotherm, kinetic and thermodynamic studies). Compos Part B: Eng 159:146–156
29. Nasseh N, Taghavi L, Barikbin B, Nasseri MA (2018) Synthesis and characterizations of a novel FeNi3/SiO2/CuS magnetic nanocomposite for photocatalytic degradation of tetracycline in simulated wastewater. J Clean Prod 179:42–54
30. Nasseh N, Taghavi L, Barikbin B, Nasseri MA, Allahresani A (2019) FeNi3/SiO2 magnetic nanocomposite as an efficient and recyclable heterogeneous fenton-like catalyst for the oxidation of metronidazole in neutral environments: Adsorption and degradation studies. Compos Part B: Eng 166:328–340
31. Nasseri MA, Sadeghzadeh SM (2013) A highly active FeNi3–SiO2 magnetic nanoparticles catalyst for the preparation of 4H-benzo [b] pyrans and Spirooxindoles under mild conditions. J Iran Chem Soc 10(5):1047–1056
32. Ojedokun AT, Bello OS (2017) Kinetic modeling of liquid-phase adsorption of Congo red dye using guava leaf-based activated carbon. Appl Water Sci 7(4):1965–1977
33. Panahi AH, Ashrafi SD, Kamani H, Khodadadi M, Lima EC, Mostafapour FK et al (2019) Removal of cephalexin from artificial wastewater by mesoporous silica materials using Box-Behnken response surface methodology. Desalin Water Treat 159:169–180
34. Prasad C, Karlapudi S, Venkateswarlu P, Bahadur I, Kumar S (2017) Green arbitrated synthesis of Fe3O4 magnetic nanoparticles with nanorod structure from pomegranate leaves and Congo red dye degradation studies for water treatment. J Mol Liq 240:322–328
35. Rahimi R, Kerdari H, Rabbani M, Shafiee M (2011) Synthesis, characterization and adsorbing properties of hollow Zn-Fe2O4 nanospheres on removal of Congo red from aqueous solution. Desalination 280(1–3):412–418
36. Rani K, Naik A, Chaurasiya RS, Raghavarao K (2017) Removal of toxic Congo red dye from water employing low-cost coconut residual fiber. Water Sci Technol 75(9):2225–2236
37. Raval NP, Shah PU, Ladha DG, Wadhwani PM, Shah NK (2016) Comparative study of chitin and chitosan beads for the adsorption of hazardous anionic azo dye Congo Red from wastewater. Desalination Water Treat 57(20):9247–9262
38. Raval NP, Shah PU, Shah NK (2016) Adsorptive amputation of hazardous azo dye Congo red from wastewater: a critical review. Environ Sci Pollut Res 23(15):14810–14853

39. Solisio C, Aliakbarian B (2017) Methylene blue adsorption using chabazite: Kinetics and equilibrium modelling. Can J Chem Eng 95(9):1760–1767
40. Somayajula A, Asaithambi P, Susree M, Matheswaran M (2012) Sonoelectrochemical oxidation for decolorization of Reactive Red 195. Ultrason Sonochem 19(4):803–811
41. Tahir Z, Malik S, Mehmood M (2016) Adsorption studies of reactive red 195 dye using modified rice husk. Sci Int (LAHORE) 28:951–954
42. Tan KA, Morad N, Teng TT, Norli I, Panneerselvam P (2012) Removal of cationic dye by magnetic nanoparticle (Fe3O4) impregnated onto activated maize cob powder and kinetic study of dye waste adsorption. APCBEE Procedia 1:83–89
43. Tang R, Dai C, Li C, Liu W, Gao S, Wang C (2017) Removal of methylene blue from aqueous solution using agricultural residue walnut shell: equilibrium, kinetic, and thermodynamic studies. Journal of Chemistry 2017
44. Taqui SN, Yahya R, Hassan A, Nayak N, Syed AA (2017) Development of sustainable dye adsorption system using nutraceutical industrial fennel seed spent—studies using Congo red dye. Int J Phytoremediation 19(7):686–694
45. Wang H, Maiyalagan T, Wang X (2012) Review on recent progress in nitrogen-doped graphene: synthesis, characterization, and its potential applications. ACS Catal 2(5):781–794
46. Wang P, Yan T, Wang L (2013) Removal of Congo red from aqueous solution using magnetic chitosan composite microparticles. BioResources 8(4):6026–6043
47. Wanyonyi WC, Onyari JM, Shiundu PM (2014) Adsorption of Congo red dye from aqueous solutions using roots of Eichhornia crassipes: kinetic and equilibrium studies. Energy Procedia 50:862–869
48. Yaman C, Gündüz G (2015) A parametric study on the decolorization and mineralization of CI Reactive Red 141 in water by heterogeneous Fenton-like oxidation over FeZSM-5 zeolite. J Environ Health Sci Eng 13(1):1–12
49. Zhu N, Ji H, Yu P, Niu J, Farooq M, Akram MW et al (2018) Surface modification of magnetic iron oxide nanoparticles. Nanomaterials 8(10):810

Figures

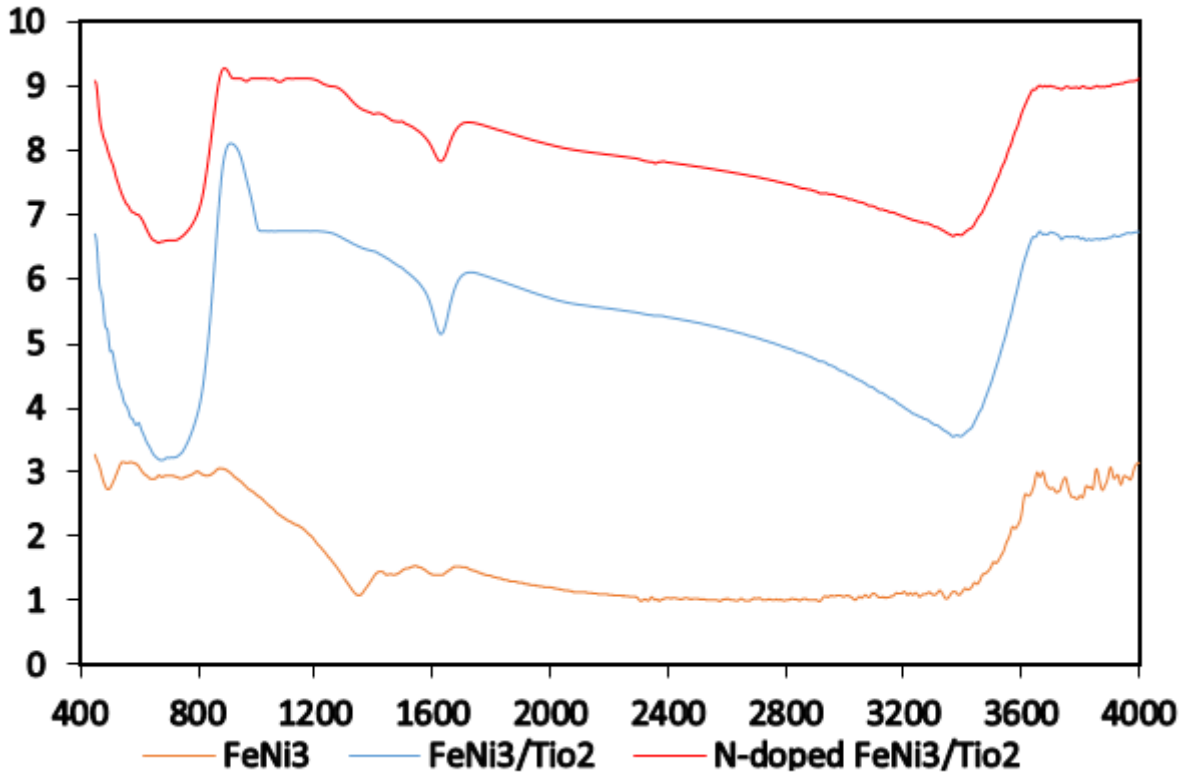

Figure 1

FTIR spectroscopy of N-doped $FeNi_3/Tio_2$ magnetic nanocomposite

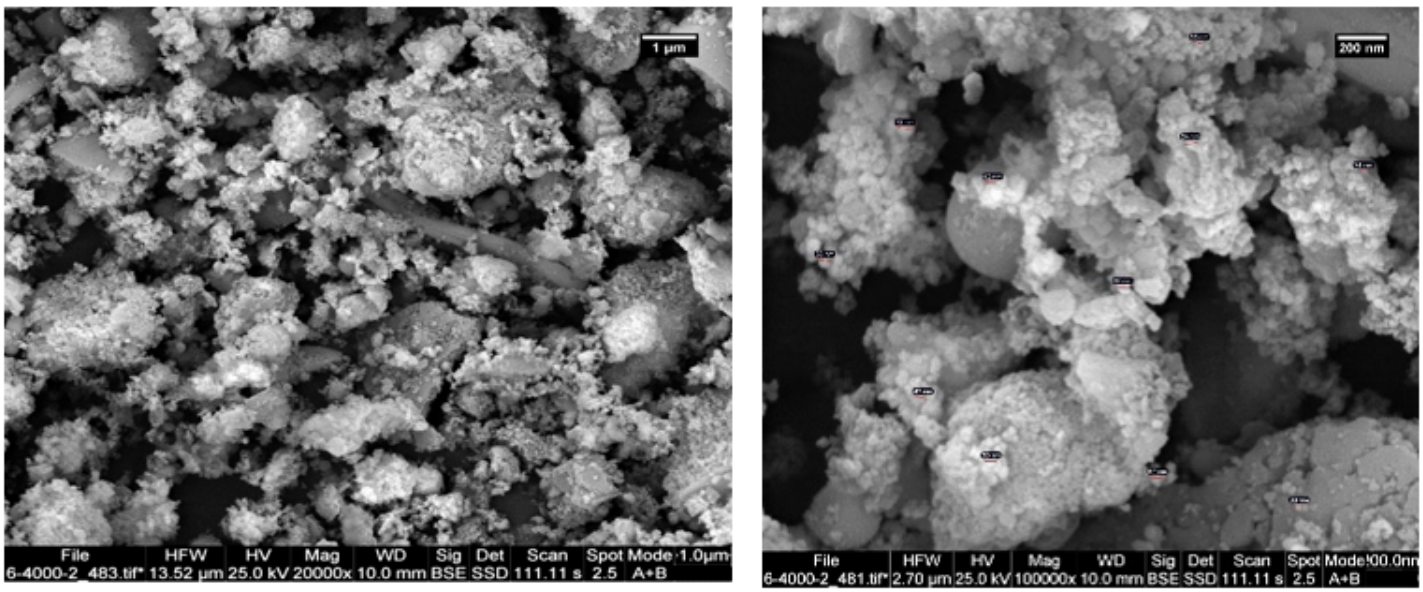

Figure 2

FESEM spectrum of N-doped $FeNi_3/Tio_2$ magnetic nanocomposite

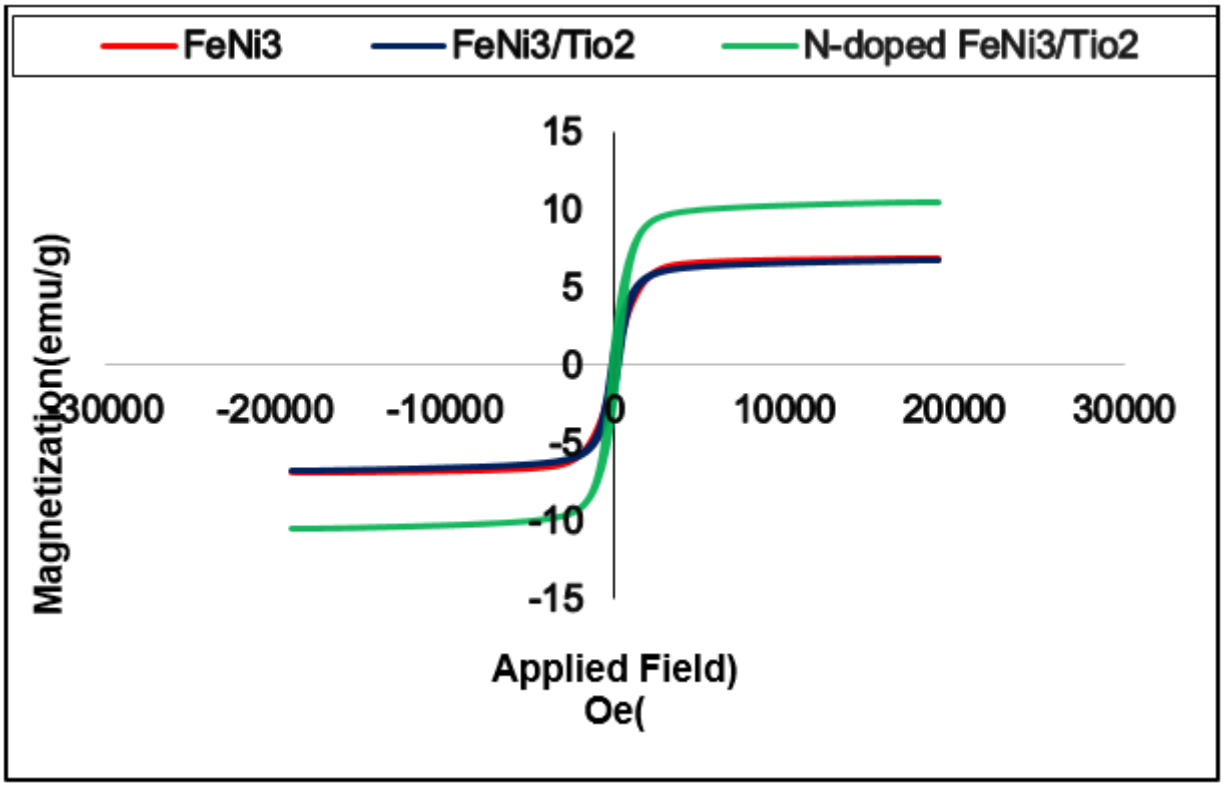

Figure 3

VSM spectrum of $FeNi_3/Tio_2$ N-doped magnetic nanocomposite

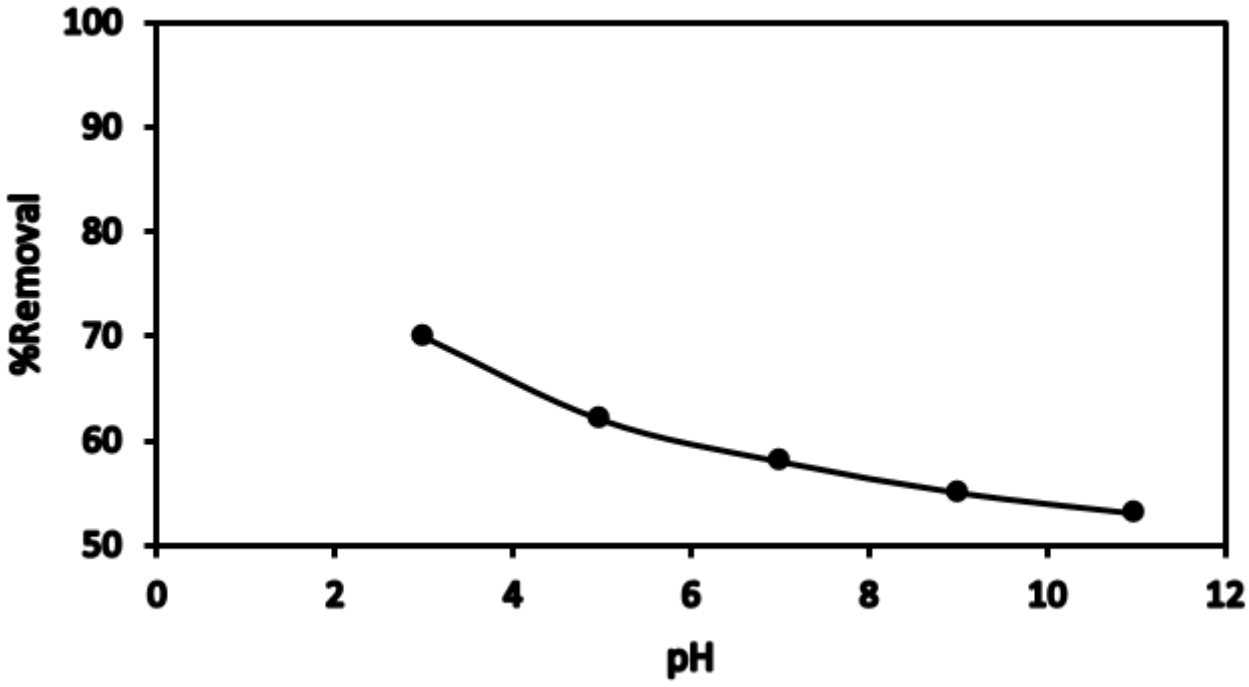

Figure 4

Effect of pH changes on reactive red 195 dye adsorption efficiency by N-doped FeNi3/Tio2 magnetic nanocomposite (RR195 initial concentration of 20 ppm, adsorbent dose of 2g L^{-1}, time of 60 minutes)

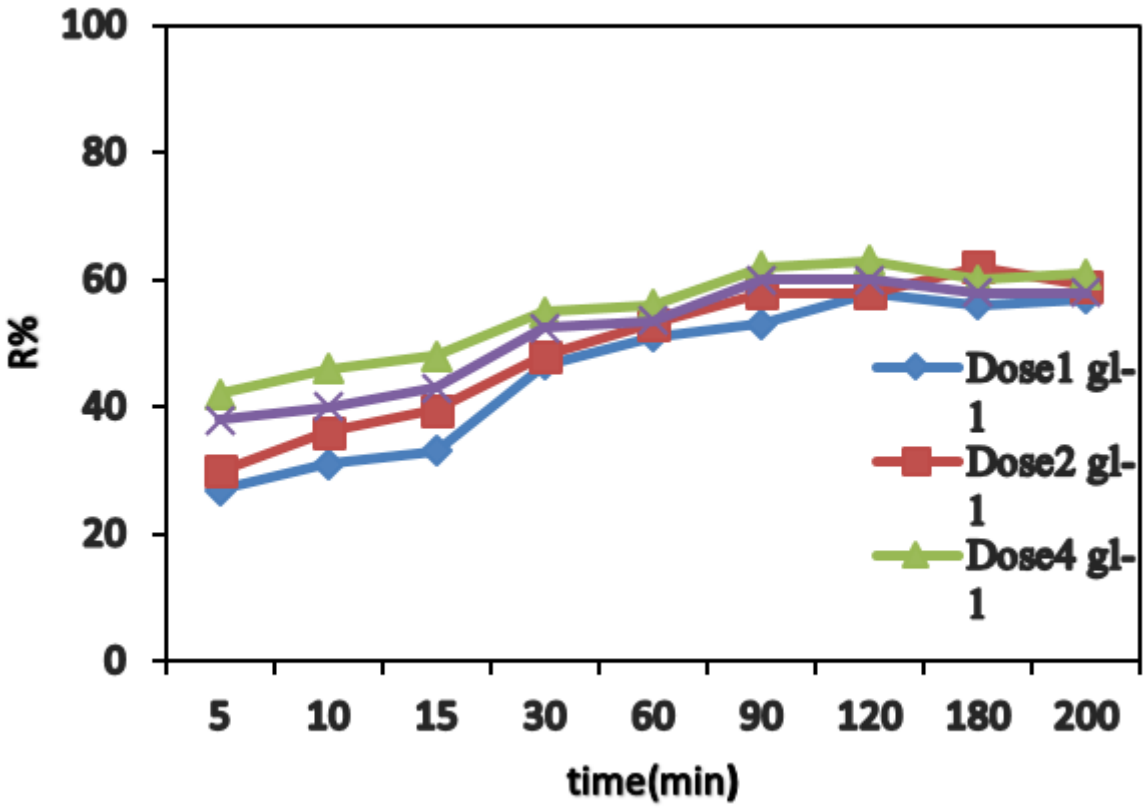

Figure 5

Effect of adsorbent dose on the removal efficiency of reactive 195red dye by N-doped FeNi3/Tio2 (pH = 3, RR195 concentration equal= 20 ppm, speed =250 rpm)

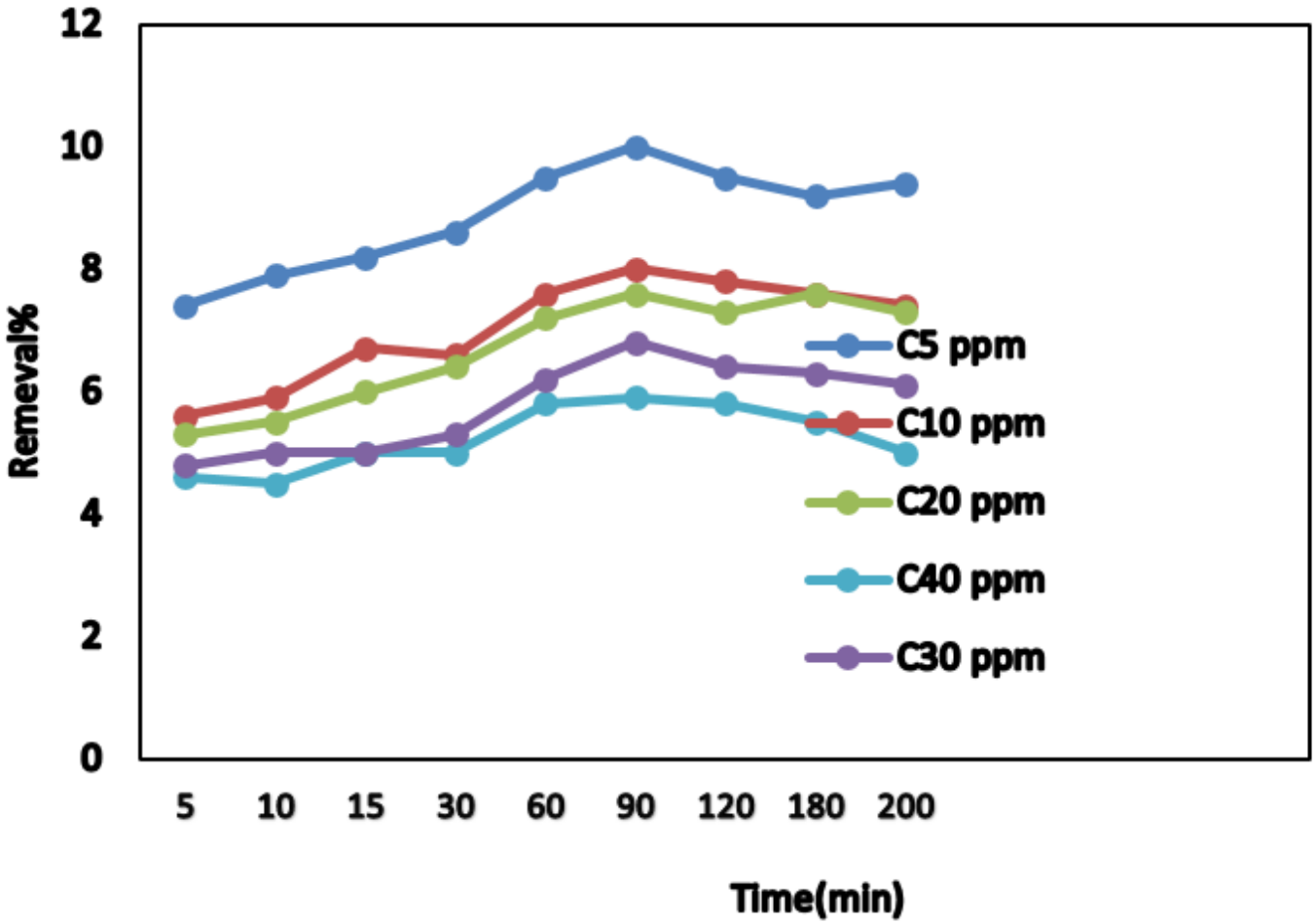

Figure 6

Initial concentration of reactive 195red dye by N-doped FeNi3/Tio2 on dye adsorption efficiency (pH = 3, adsorbent dose g $100mL^{-1}$ 4.)

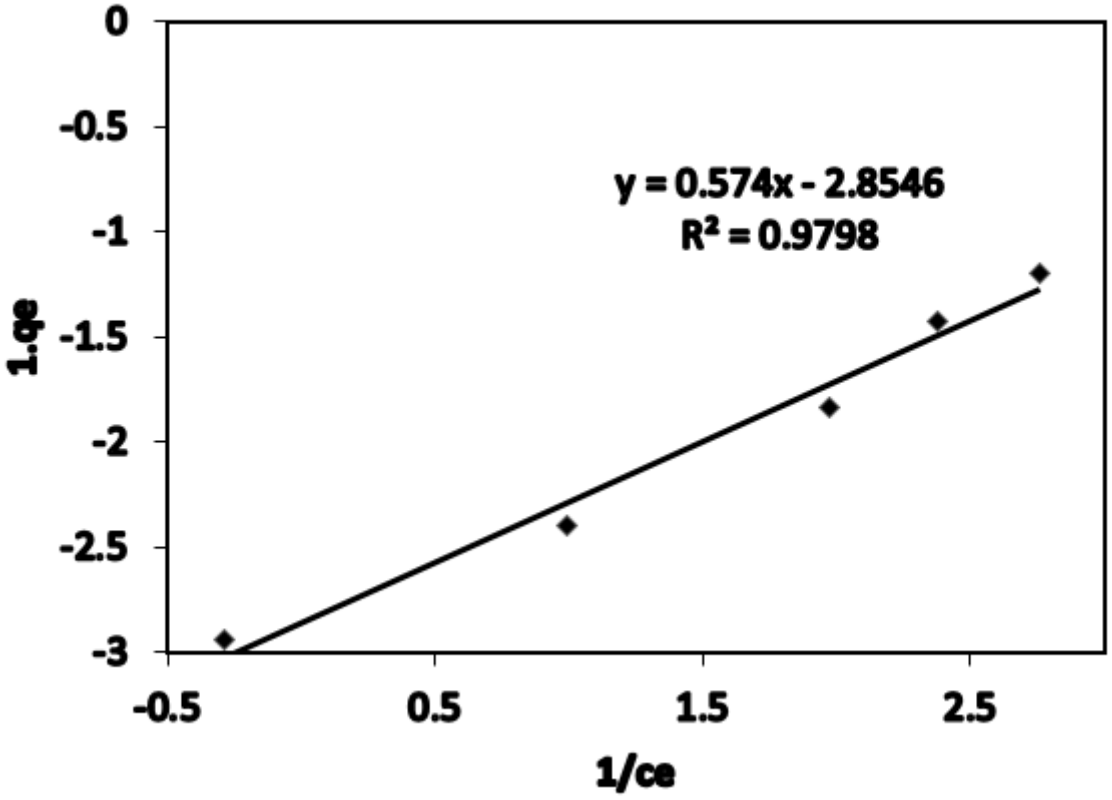

Figure 7

Investigation of Langmuir isotherm model on the adsorption of reactive red 195 using N-doped $FeNi_3/Tio_2$ magnetic nanocomposite

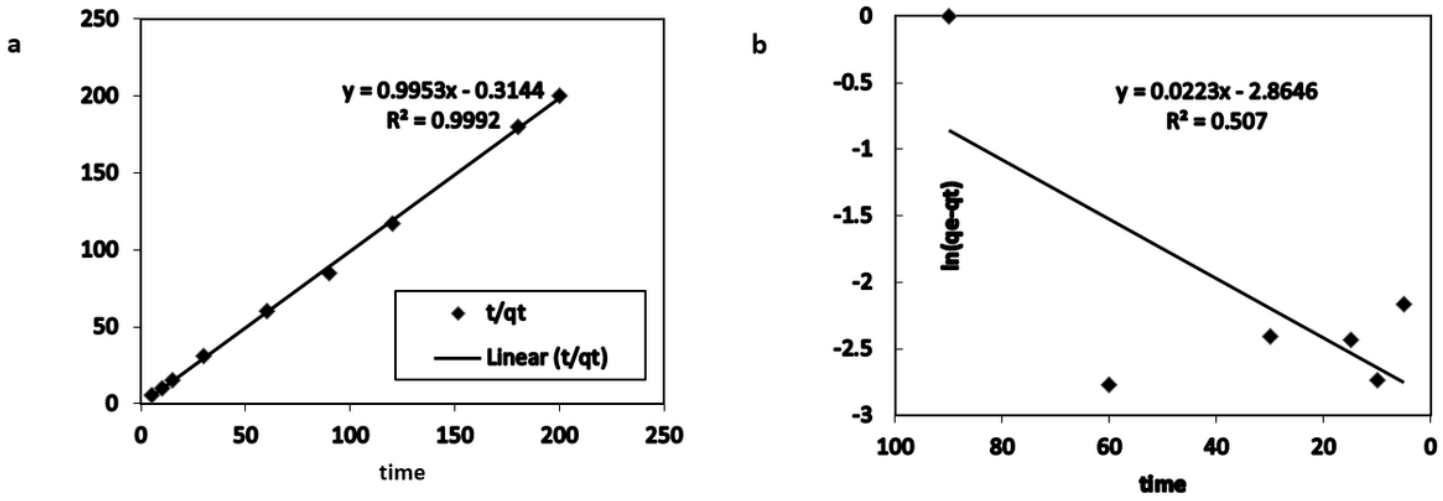

Figure 8

(a)Investigation of pseudo-second-order (b) pseudo-first-order equation kinetics using N-doped $FeNi_3/Tio_2$ magnetic nanocomposite

Supplementary Files

This is a list of supplementary files associated with this preprint. Click to download.

- GraphicalAbstract.png